Determination of the Correct Composition of "Hydrous Lead(II) Oxotellurate(IV)" as PbTeO$_3$, Crystallizing as a New Polymorph

Matthias Weil [1,*] **, Mahdi Shirkhanlou** [1] **, Ekkehard Füglein** [2] **and Eugen Libowitzky** [3]

[1] Institute for Chemical Technologies and Analytics, Division of Structural Chemistry, TU Wien, Getreidemarkt 9/164-SC, A-1060 Vienna, Austria; e1128251@student.tuwien.ac.at
[2] NETZSCH-Gerätebau GmbH, Wittelsbacherstraße 42, D-95100 Selb, Germany; Ekkehard.Fueglein@netzsch.com
[3] Institute for Mineralogy and Crystallography, Faculty of Geosciences, Geography and Astronomy, Althanstr. 14, A-1090 Vienna, Austria; eugen.libowitzky@univie.ac.at
* Correspondence: Matthias.Weil@tuwien.ac.at; Tel.: +43-01-58801-17122

Abstract: In previous studies, it has been reported that the crystalline product precipitated from the reaction of aqueous solutions of lead(II) salts with sodium oxotellurate(IV) is hydrous lead(II) oxotellurate(IV); however, there have been conflicting specifications of the water content, and the crystal structure of the product is yet undetermined. During the present study, it was shown that the precipitated material does not contain any structural water and in fact represents the third modification (denoted as γ-) of PbTeO$_3$, as revealed by thermal analysis, vibrational spectroscopy, single crystal and powder X-ray diffraction. This modification crystallizes in the space group $P\bar{1}$ with five formula units in the asymmetric unit, comprising off-centred coordination polyhedra around the Pb^{II} cations (coordination numbers: 5–7 with Pb-O distances ranging from 2.3–3.0 Å), and trigonal-pyramidal TeO$_3^{2-}$ units. The thermal behaviour and structural phase transitions of PbTeO$_3$ were investigated by means of temperature-dependent X-ray powder diffraction and complementary thermal analysis measurements. In addition, the crystal structure of β-PbTeO$_3$ was redetermined, and a comparison was made between the three known polymorphs of PbTeO$_3$.

Keywords: structure determination; lead(II) oxotellurate(IV); polymorphism; thermal behaviour; thermal analysis; vibrational spectroscopy

1. Introduction

The structures of lead(II) compounds are characterized by the presence of the 6s^2 free electron pair E that in the majority of cases is stereochemically active [1], and hence enforces an asymmetrical coordination around the lead(II) cation. In some cases, the resulting off-centred polyhedra with either holo- or hemidirected ligands [2] are made responsible for the formation of crystal structures without an inversion centre—a pre-condition for physical phenomena like piezoelectricity or non-linear optical properties. Moreover, materials with non-centrosymmetric *and* polar structures are qualified to show pyroelectricity or ferroelectricity. Thus, compounds containing atoms and/or ions with ns^2 free electron pairs are predestined to fulfil the mentioned crystallographic criteria. For example, lead(II) oxotellurate(IV) that actually contains two different building units with free electron pairs (viz. the Pb^{II} cation and the Te^{IV}O$_3^{2-}$ anion) is reported to show non-linear optical properties [3] for one of its polymorphic forms, crystallizing in the polar space group $P4_1$ [4]. This polymorph is denoted as the β-form for the following discussion. The other structurally determined PbTeO$_3$ polymorph has a centrosymmetric crystal structure [5,6] and is denoted as the α-form. Other (mineral) phases with

composition $PbTeO_3$ are claimed to have triclinic symmetry (mineral fairbankite [7]) and orthorhombic symmetry (mineral plumbotellurite [8]), however, both without structural proof. In addition, another cubic phase is reported for this composition [9]. Apart from the missing information with respect to the crystal structures and possible phase transitions of the latter three phases, another aspect makes $PbTeO_3$ or other compounds in the ternary system Pb/Te/O [9–12] interesting because they may occur as unwanted surfacial oxidation products of lead telluride, PbTe. The latter is a well-known narrow gap semiconductor and a thermoelectric material for mid-range temperature (600–800 K) applications [13]. In fact, oxidation products of bulk PbTe were analysed by secondary ion mass spectrometry and reported to be $PbTeO_3$ phases [14]. Such phases were also identified by X-ray powder diffraction for PbTe quantum dots embedded in glass matrices under heat-treatment [15], whereas the formation of crystalline surfacial oxidation products could not be found for PbTe core–shell nanostructures, although an incorporation of oxygen on the surface was clearly shown by energy dispersive X-ray spectroscopy [16]. Hence, structural knowledge of all possible phases in the Pb/Te/O system and details with respect to their formation conditions are highly desirable.

A convenient method for the synthesis of (metastable) compounds makes use of the "chimie douce" approach under relatively mild conditions [17]. Similar to the formation of the metastable phase ε-$SrTeO_3$ by dehydration of $SrTeO_3(H_2O)$ at temperatures above 150 °C [18], we started to investigate the structural and thermal characteristics of the reported hydrous phase $PbTeO_3 \cdot x(H_2O)$ which can be easily obtained by precipitation from aqueous solutions. Although working under similar preparative conditions, the molar water content x of this phase has either been determined to be 2/3 [19], 1/3 [20], or was not reported at all because the exact composition of the hydrated form could not be determined reliably [11]. However, our current investigations revealed that the precipitated material does not contain any structural water, and in fact represents a third $PbTeO_3$ polymorph, designated in the following discussion as γ-$PbTeO_3$. The crystal structure and thermal behaviour of this material are reported in the present contribution, together with a redetermination of the crystal structure of the β-polymorph of $PbTeO_3$.

2. Experimental

2.1. Synthesis and Crystallization

Polycrystalline material was prepared by precipitation according to [19]. A diluted aqueous solution of $Pb(NO_3)_2$ (ca. 25 °C, 5%wt) was added dropwise to a warm aqueous Na_2TeO_3 solution (ca. 60 °C, 10% wt) which resulted in an immediate precipitation of a colourless flocculent material. The solid became crystalline after keeping the solution between 60 °C and 70 °C under constant stirring for several hours. The as-obtained product was filtered off, washed with mother liquor, water, and ethanol, and dried in a desiccator over $CaCl_2$ for several days. According to the subsequent structure determination on the basis of single crystal data, the precipitated material was single phase γ-$PbTeO_3$ as revealed by powder X-ray diffraction (Supplementary Figure S1).

Single crystals of γ-$PbTeO_3$ were grown by hydrothermal treatment of the precipitated material obtained as described above; 300 mg of the precipitate were loaded together with approximately 5 mL of the mother liquor in a Teflon container (capacity 10 mL). The container was sealed with a Teflon lid, placed in a steel autoclave, and heated at 210 °C for one week at autogenous pressure. The autoclave was then cooled to room temperature over the course of several hours. Colourless to light yellow translucent crystals were isolated from the reaction product. X-ray powder diffraction of the bulk revealed the oxotellurates(IV) γ-$PbTeO_3$ and $Pb_2Te_3O_8$ [21] as the main phases and the oxotellurate(VI) Pb_2TeO_5 [22] as a minority phase. Some additional reflections could not be assigned to any known phase(s).

It should be noted that single crystals of both β- and γ-$PbTeO_3$ polymorphs were also obtained occasionally during hydrothermal phase formation studies in the presence of other elements. For example, γ-$PbTeO_3$ single crystals were identified as a minority phase under very similar conditions as described above, with CuO (80 mg), PbO (225 mg), and H_6TeO_6 (226 mg) in a stoichiometric ratio

of 1:1:1 as starting materials, while β-PbTeO$_3$ crystals appeared (also as a minority phase) after hydrothermal reaction of Pb(NO$_3$)$_2$ (267 mg), TeO$_2$ (84 mg), H$_2$SeO$_4$ (0.17 mL), and NaOH (64 mg) in a stoichiometric ratio of 1.5:1:2:3.

2.2. X-ray Powder Diffraction (XRPD)

Samples of the bulk material were ground, fixed with small amounts of petroleum jelly on silicon wafers, and measured with Cu-K$\alpha_{1,2}$ radiation in Bragg–Brentano geometry on a PANalytical X'PertPro diffractometer (PANAlytical, Almelo, The Netherlands). The system has been recently calibrated with NIST LaB$_6$ standard; X'Celerator multi-channel detector; 2.546° scan length; 25 s exposure time per scan length; 2θ range 5°–70°; the scans were finally converted into 0.02° step-size bins. For temperature-dependent measurements of γ-PbTeO$_3$ up to a maximum temperature of 525 °C, a HTK1200 Anton-Paar oven chamber was mounted on the diffractometer. The finely ground polycrystalline material was placed on a glass ceramic (Marcor®) sample holder with 0.5 mm depth. The zero point was automatically adjusted during the measurements with a PC-controllable alignment stage. The sample was heated to the respective temperature under vacuum (10^{-2} bar) at a rate of 5 °C/min and kept for 15 min before measurement of each step to ensure temperature-stability.

2.3. Single Crystal Diffraction

Crystals of both β- and γ-PbTeO$_3$ modifications were preselected under a polarising microscope, embedded in perfluorinated polyether, and then mounted on MiTeGen MicroLoops^{TM}. The crystals with the best performance in terms of reflection intensity and reflection shape were eventually used for room-temperature data collection on a Bruker APEX-II CCD diffractometer (Bruker-AXS, Madison, WI, USA) with Mo-Kα radiation, using narrow ω- and ϕ-scans (0.5° frame widths). In each case, data collection strategies were optimized with APEX-2 [23], resulting in highly redundant data sets that were subsequently reduced with SAINT [23]. The crystal structures of β- and γ-PbTeO$_3$ were solved by Direct Methods and refined using the SHELXTL program package [24]. An absorption correction for γ-PbTeO$_3$ based on optimisation of the crystal form was performed on eight crystal faces of the block-shaped crystal using the program HABITUS [25]. An absorption correction of the irregularly-shaped crystal of β-PbTeO$_3$ was based on the multi-scan approach with SADABS [23]. The remaining electron density peaks (maximum/minimum values $\approx$ 2.5 e$^-$/Å^3) were unobstrusive and characteristic of truncation effects around the heavy atoms. Numerical details of the data collections and structure refinements are gathered in Table 1. Selected bond lengths and angles are collated in Table 2, together with the results of bond valence sum (BVS) calculations [26], given in valence units (v.u.). For this purpose, values of R_0 = 1.963, B = 0.49 for Pb–O interactions [27], as well as R_0 = 1.917, B = 0.37 for Te–O interactions [28] were used.

Further details of the crystal structure investigation may be obtained from the Fachinformationszentrum Karlsruhe, 76344 Eggenstein-Leopoldshafen, Germany (Fax: +49-7247-808-666; E-Mail: crysdata@fiz-karlsruhe.de, https://www.fiz-karlsruhe.de) on quoting the depository numbers listed at the end of Table 1. Drawings of structural details were produced using the program ATOMS [29].

2.4. Vibrational Spectroscopy

A Bruker Tensor 27 Fourier transform infrared (FTIR) spectrometer combined with a Harrick MVP2 Series diamond attenuated total reflection (ATR) accessory was used for recording ATR spectra in the 4000$-$480 cm^{-1} region. The instruments were equipped with a glo(w)bar IR source, a KBr beam splitter, and a DLaTGS detector. The spectra were collected with a 4 cm^{-1} spectral resolution and averaged over 32 scans of the background and the sample. Raman spectra were collected by using a Renishaw RM 1000 micro-Raman system in the spectral range from 4000 to 40 cm^{-1}. The 632.8 nm excitation line of a 17 mW HeNe laser was focused with a 50 $\times$ 0.75 objective on the sample surface. Raman intensities were collected with a thermoelectrically-cooled CCD array detector. The resolution of the system was 4 cm^{-1}, the wave number accuracy was $\pm$1 cm^{-1}, both calibrated with the Rayleigh line and the 520.5 cm^{-1} line of a Si standard.

Table 1. Details of data collections, structure solutions, and refinements.

Formula	PbTeO$_3$	
Modification	γ-	β-
Diffractometer	Bruker APEX-II CCD	
Radiation; wavelength/Å	Mo K$\bar{a}$; 0.71073	
Temperature/°C	22(1)	
Formula weight	382.79	
Space group (No.)	$P\bar{1}$ (2)	$P4_1$ (76)
Crystal description	colourless block	colourless fragment
Crystal dimensions/mm^3	0.022 × 0.034 × 0.045	0.060 × 0.080 × 0.080
Formula units Z	10	4
a/Å	7.0185(3)	5.3193(6)
b/Å	10.6166(4)	
c/Å	11.9616(5)	11.9326(15)
α/°	78.548(3)	
β/°	82.992(2)	
γ/°	84.048(2)	
Volume/Å^3	864.12(6)	337.63(9)
μ/mm^{-1}	56.887	58.238
X-ray density/g·cm^{-3}	7.356	7.531
Rangeθ_{min}–θ_{max}/°	1.75 → 41.40	3.83 → 29.98
Range h; k; l	−11 → 13; −19 → 19; −22 → 22	−7 → 7; −5 → 7; −16 → 16
Measured reflections	61288	3495
Independent reflections	11367	976
Observed reflections [$I > 2\sigma(I)$]	6799	622
R_i	0.075	0.034
Absorption correction	numerical, HABITUS [25]	numerical, SADABS [23]
Coef. Of Transmission T_{min}; T_{max}	0.177; 0.409	0.383; 0.750
Structure solution and refinement	SHELXTL [24]	
Number of parameters	227	46
Extinction coefficient (SHELXTL)	0.000504(5)	-
Absolute structure parameter		Flack x = −0.017(6)
Difference electron density/e·Å^{-3}, with distance to atom/Å	$\Delta\rho_{max}$ = 2.41 [0.67; Pb3]; $\Delta\rho_{min}$ = −2.53 [0.48; Pb2]	$\Delta\rho_{max}$ = 1.03 [1.14; O3]; $\Delta\rho_{min}$ = −2.52 [0.68; Pb1]
$R[F^2 > 2\sigma(F^2)]$; w$R(F^2$ all)	0.0289; 0.0360	0.0301; 0.0722
Goof	0.653	1.037
CSD number	432744	432745

2.5. Thermal Analysis

The γ-PbTeO$_3$ powder samples were investigated as-synthesised, without special treatment (e.g., by equilibration at certain humidity). A simultaneous thermal analyser NETZSCH STA 449 *F5 Jupiter* (Netzsch, Selb, Germany) with silicon carbide furnace was used to investigate the temperature-dependent behaviour of γ-PbTeO$_3$ with simultaneous thermogravimetry (TG) and differential thermal analysis (DTA). The TG-DTA-sample carrier (type S) allows for detection of both caloric effects as well as mass changes. First, 14.842 mg γ-PbTeO$_3$ were transferred into an open aluminium pan and heated at a 10 °C/min heating rate from ambient temperature to 500 °C. The successive cooling was carried out at 10 °C/min down to 200 °C. During heating and cooling, the sample was purged with argon (5.0) using a total purge gas flow rate of 70 mL/min.

Differential scanning calorimetry (DSC) measurements were performed on a NETZSCH DSC 204 *F1 Phoenix* (Netzsch, Selb, Germany) instrument to study γ-PbTeO$_3$ with respect to the reversibility of its caloric transitions. Sample amounts of 10.0 ($\pm$0.5) mg were transferred into aluminium pans with pierced lids. The samples were heated and cooled between 30 °C and 590 °C with heating and cooling rates of 20 °C/min. A total purge gas flow rate of 40 mL/min nitrogen (5.0) served for an inert sample environment.

3. Results and Discussion

3.1. Crystal Structures of the PbTeO$_3$ Polymorphs—General Features

The three modifications of PbTeO$_3$ all comprise isolated oxotellurate(IV) anions, TeO$_3{}^{2-}$, with the characteristic trigonal-pyramidal shape. This type represents the most frequently observed coordination polyhedron of oxotellurates(IV) for which four- and five-coordinated Te^{IV} atoms are also known [30,31]. The three Te–O bonds have lengths between 1.85 and 1.92 Å and three O–Te–O bond angles between 90° and 102°. Like for most oxotellurates(IV), the $5s^2$ lone electron pair of the Te^{IV} atom is stereochemically active in the three modifications, and points to the empty space in the crystal structures. This stereochemical activity is also observed for the Pb^{II} cations in the three polymorphs, but each with a different bond lengths distribution and variable coordination numbers. As a threshold for the definition of the first coordination sphere of the Pb^{II} cations in the crystal structures of the lead(II) oxotellurates(IV), we used a Pb–O bond length of 3.55 Å. This value is based on the sum of the van der Waals radii of Pb and O (2.02 and 1.52 Å, respectively [32]) and on BVS calculations, because a Pb^{II}–O bond of 3.5 Å still accounts for 2.2% of the overall BVS. Given the broad Pb–O bond lengths distribution between 2.3 and 3.6 Å in the crystal structures (Table 2), it is useful to subdivide Pb–O bonds into "short" bonds less than 2.8 Å and "long" bonds greater than this boundary. As can be evidenced from the results of BVS calculations, it is clear that the contributions of "long" Pb–O bonds cannot be neglected. Only if these "long" bonds are included do the BVS at some of the Pb and O sites raise to much more reasonable values. For the sake of clarity, crystal structure plots depict only "short" Pb–O bonds up to 2.80 Å, whereas individual [PbO$_x$] polyhedra are shown with all relevant Pb–O contacts, distinguishing short Pb–O distances with filled and long Pb–O distances with open bonds, respectively.

The determined X-ray densities and the corresponding V/Z ratios (V = crystal volume/Å^3; Z = number of formula units) of the three PbTeO$_3$ modifications are markedly different, which we ascribe to packing effects in the three modifications: α-PbTeO$_3$ [6], 7.28 g cm^{-3}, 87.28 Å^3; β-PbTeO$_3$ [this work], 7.53 g cm^{-3}, 84.41 Å^3; γ-PbTeO$_3$ [this work], 7.36 g cm^{-3}, 86.41 Å^3. Following the general rule that the densest phase of a polymorphic compound also represents (in the majority of cases) the thermodynamically stable phase reveals the β-polymorph to be the thermodynamically stable phase at room temperature, and the α- and γ-polymorphs as metastable phases. The same conclusion was drawn [11] from repeated melting and recrystallisation experiments of mixtures with nominal composition PbO·TeO$_2$ (more precisely, only for the metastable α- and stable β-polymorphs, because the γ-polymorph was thought to be a hydrated phase at that time).

3.2. Crystal Structures of the PbTeO$_3$ Polymorphs

γ-PbTeO$_3$ crystallizes in the space group $P\bar{1}$ and comprises five formula units in the asymmetric unit (Pearson symbol $aP30$). The coordination numbers of the five Pb^{II} cations range from 5 to 7, associated with very distorted and "one-sided" (or "off-centred") coordination spheres for each of the Pb^{II} cations. Pb1 is surrounded by five oxygen atoms (Pb–O range 2.30–2.68 Å), Pb2 by seven (with five O atoms within the 2.80 Å boundary and two outside, i.e., a [5+2] coordination; overall Pb–O range 2.31–2.95 Å), Pb3 by seven ([6+1]; 2.41–2.84 Å), Pb4 by six (2.37–2.74 Å), and Pb5 by five (2.32–2.76 Å) O atoms (Figure 1a, Table 2).

Table 2. Selected interatomic distances/Å and angles/° , as well as results from BVS calculations/v.u. [1] .

γ-PbTeO₃								
Pb1	–	O1	2.293(3)	Te1	–	O6	1.868(3)	
Pb1	–	O12	2.366(3)	Te1	–	O3	1.872(3)	
Pb1	–	O14	2.387(3)	Te1	–	O2	1.903(3)	
Pb1	–	O7	2.485(3)	Te2	–	O15	1.851(3)	
Pb1	–	O13	2.673(3)	Te2	–	O10	1.882(3)	
Pb2	–	O2	2.309(3)	Te2	–	O12	1.885(3)	
Pb2	–	O12	2.527(3)	Te3	–	O14	1.863(3)	
Pb2	–	O2	2.540(3)	Te3	–	O7	1.872(3)	
Pb2	–	O14	2.571(3)	Te3	–	O11	1.875(3)	
Pb2	–	O15	2.624(4)	Te4	–	O13	1.866(3)	
Pb2	–	O11	2.916(3)	Te4	–	O8	1.871(3)	
Pb2	–	O15	2.948(4)	Te4	–	O9	1.919(3)	
Pb3	–	O8	2.405(3)	Te5	–	O5	1.868(3)	
Pb3	–	O3	2.470(3)	Te5	–	O4	1.872(3)	
Pb3	–	O9	2.484(3)	Te5	–	O1	1.900(3)	
Pb3	–	O7	2.549(3)					
Pb3	–	O13	2.729(3)			O6–Te1–O3	98.43(14)	
Pb3	–	O1	2.748(3)			O6–Te1–O2	90.87(13)	
Pb3	–	O10	2.837(3)			O3–Te1–O2	99.32(13)	
Pb4	–	O4	2.366(3)			O15–Te2–O10	97.23(14)	
Pb4	–	O10	2.457(3)			O15–Te2–O12	101.14(16)	
Pb4	–	O5	2.505(3)			O10–Te2–O12	98.19(15)	
Pb4	–	O8	2.558(3)			O14–Te3–O7	100.31(14)	
Pb4	–	O6	2.561(3)			O14–Te3–O11	97.59(14)	
Pb4	–	O5	2.736(3)			O7–Te3–O11	96.61(14)	
Pb5	–	O11	2.320(3)			O13–Te4–O8	102.54(13)	
Pb5	–	O9	2.334(3)			O13–Te4–O9	96.33(13)	
Pb5	–	O6	2.363(3)			O8–Te4–O9	97.58(14)	
Pb5	–	O3	2.446(3)			O5–Te5–O4	97.42(14)	
Pb5	–	O4	2.755(3)			O5–Te5–O1	101.38(13)	
						O4–Te5–O1	95.96(13)	

BVS. Pb1 1.95, Pb2 1.94, Pb3 1.99, Pb4 1.93, Pb5 1.96, Te1 3.89, Te2 3.98, Te3 4.02, Te4 3.85, Te5 3.90, O1 (1 Te, 2 Pb) 1.95, O2 (1 Te, 2 Pb) 2.02, O3 (1 Te, 2 Pb) 2.06, O4 (1 Te, 2 Pb) 1.96, O5 (1 Te, 2 Pb) 1.88, O6 (1 Te, 2 Pb) 2.08, O7 (1 Te, 2 Pb) 1.98, O8 (1 Te, 2 Pb) 2.03, O9 (1Te, 2Pb) 1.98, O10 (1 Te, 2 Pb) 1.83, O11 (1 Te, 2 Pb) 1.95, O12 (1 Te, 2 Pb) 2.03, O13 (1 Te, 2 Pb) 1.98, O14 (1 Te, 2 Pb) 2.08, O15 (1 Te, 2 Pb) 1.80.

β-PbTeO₃								
Pb1	–	O3	2.245(8)	Te1	–	O1	1.877(8)	
Pb1	–	O1	2.427(9)	Te1	–	O3	1.877(8)	
Pb1	–	O2	2.510(9)	Te1	–	O2	1.883(8)	
Pb1	–	O2	2.604(8)					
Pb1	–	O1	2.698(9)			O1–Te1–O3	95.3(4)	
Pb1	–	O3	2.703(10)			O1–Te1–O2	98.8(4)	
Pb1	–	O3	3.545(8)			O3–Te1–O2	103.8(4)	

BVS. Pb1 1.99, Te1 3.91, O1 1.92 (1 Te, 2 Pb) O2 1.89 (1 Te, 2 Pb) O3 2.09 (1 Te, 2 Pb).

(1) For oxygen atoms, the type and number of atoms they are bound to are indicated in parentheses.

The various [PbOₓ] polyhedra share edges and corners to build up a three-dimensional framework. The five Te^{IV} atoms are situated in the free space of the lead-oxygen framework. They are bound to three oxygen atoms each, forming isolated TeO₃²⁻ groups. The crystal structure of γ-PbTeO₃ can be rationalised as being composed of Pb^{II} cations and TeO₃²⁻ groups arranged in sheets parallel ($\bar{1}$10). Adjacent sheets are held together by more remote Pb–O contacts. Typical for the crystal chemistry of lead(II) and oxotellurate(IV) compounds, the corresponding lone pair electrons are stereochemically active and protrude into the remaining space in the structure (Figure 2).
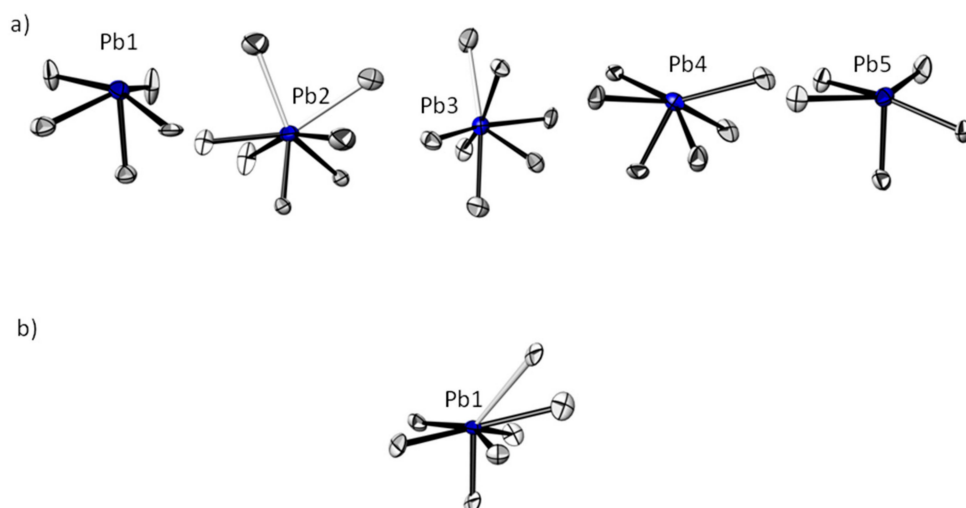
Figure 1. The coordination environments of the Pb[II] cations in the crystal structures of (**a**) γ-PbTeO$_3$ and (**b**) β-PbTeO$_3$. Pb–O bonds (<2.8 Å) are displayed with filled lines, longer bonds (2.8–3.6 Å) with open lines. Anisotropic displacement parameters are displayed at the 90% probability level.
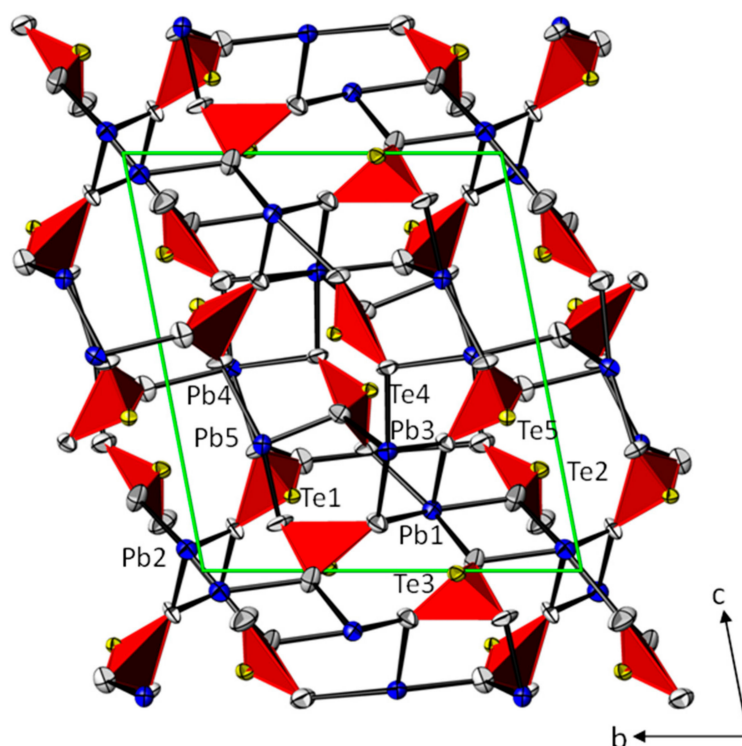

Figure 2. The crystal structure of γ-PbTeO$_3$ in a projection along [100]. TeO$_3{}^{2-}$ anions are given in polyhedral representation with Te[IV] atoms in yellow and O atoms in white. Displacement ellipsoids are as in Figure 1.

Structure determination of the new γ-modification did not reveal any incorporation of water into the crystal structure. This result was confirmed by infrared spectroscopy—in general a very reliable method to detect even small amounts of (structurally bound) water, because the characteristic OH vibrational bands in the region between 3800–3200 cm^{-1} are completely missing (Supplementary Figure S2). We interpret the small mass loss observed during thermogravimetric measurements of the precipitated material (see detailed discussion below) to desorption processes of unknown volatile

material. In general, the amount of adsorbed water depends on the preparation and crystallization conditions (surface, crystallinity, etc.), which might explain the different reported specifications of the water content of precipitated $PbTeO_3$ samples—i.e., 2/3 mole per formula unit [19], 1/3 mole per formula unit [20], or an undetermined amount of water [11].

The current redetermination of the β-$PbTeO_3$ structure confirms the original structure model [4] in the polar space group $P4_1$, but with higher accuracy and precision. In contrast to the previous refinement, all atoms were refined with anisotropic displacement parameters, and the absolute structure was determined by using 207 quotients $[(I+) - (I-)]/[(I+) + (I-)]$ [33] (Table 1). β-$PbTeO_3$ crystallizes with one formula unit in the asymmetric unit of the primitive tetragonal unit cell (Pearson symbol $tP20$). A pronounced I-centred tetragonal subcell is present in the crystal structure if only the heavy atoms Pb and Te are considered. Weak but clearly discernible superstructure reflections break the I-centring, and the lattice becomes primitive.

The coordination number of the unique Pb^{II} cation is six with a Pb–O bond length range of 2.25–2.70 Å. The next-nearest O atom is located 3.545(8) Å from the Pb^{II} cation, and is on the outer limit to be considered as bonding (see above). Again, the coordination sphere of the Pb^{II} cation shows a distinct "one-sided" shape and might be described as a distorted pentagonal pyramid if only the strong interactions are considered (Figure 1b), with the $6s^2$ electron lone-pair pointing towards the direction opposite to the apical O3 atom. The latter O atom exhibits the shortest of all Pb–O distances. In the crystal, the linkage of the $[PbO_6]$ polyhedra through edge- and corner-sharing sets up a three-dimensional framework with channels extending parallel to [001] into which the electron lonepairs of the Pb^{II} cations are arranged. In a channel, the Te^{IV} atoms are situated at approximately the same height as opposite Pb^{II} cations at $z \approx 0, \frac{1}{4}, \frac{1}{2}, \frac{3}{4}$ and bridge three O atoms of the lead-oxygen framework in a trigonal-pyramidal configuration. The $5s^2$ lone pair of the Te^{IV} atom is likewise oriented towards the open space of the channel, the diameter of which is $\approx$3.8 Å (Figure 3).

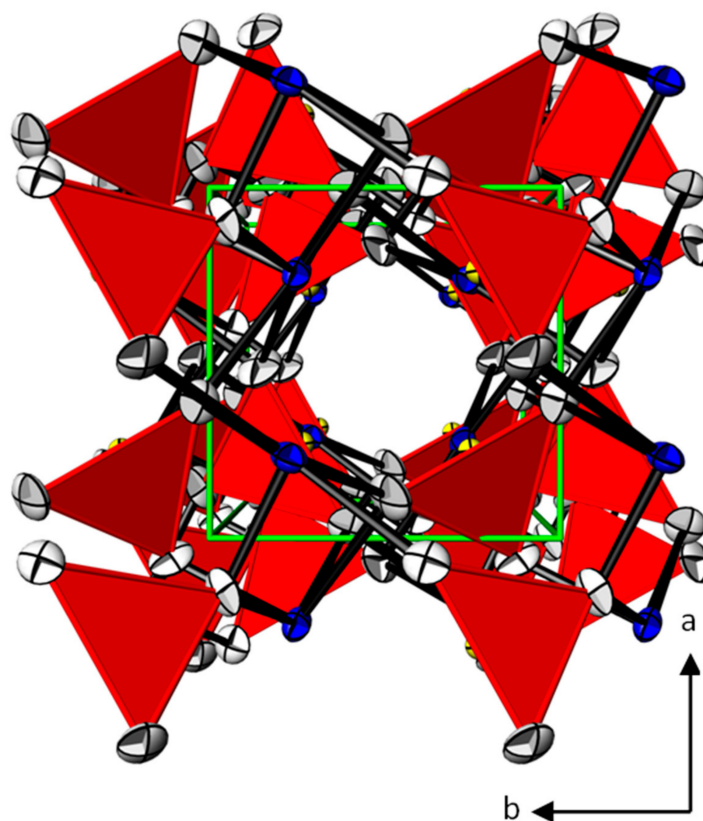**Figure 3.** The crystal structure of β-$PbTeO_3$ in a perspective view along [001]. Colour codes and displacement ellipsoids are as in Figure 2.

α-PbTeO$_3$ crystallizes in the monoclinic space group $C2/c$ [5,6] with $Z = 24$ (Pearson symbol $mC120$). The asymmetric unit of this modification comprises three formula units. The three Pb^{II} cations exhibit coordination numbers of 9 (Pb1, Pb2) and 7 (Pb3), with a Pb–O bond lengths range between 2.25–3.27 Å. Using the 2.8 Å threshold for "short" bonds, the coordination spheres of the three Pb^{II} cations can be classified as [5+4], [4+5], and [4+3], respectively. The three lead-oxygen polyhedra are linked through corners, edges, and faces to form a three-dimensional framework with channels propagation parallel to [010]. The three Te^{IV} atoms are located on the outer boundary of the channels. Each of these is coordinated trigonal-pyramidally by three O atoms from the framework, with the electron lone pairs pointing away from the channel into the remaining free space of the channels (Figure 4).
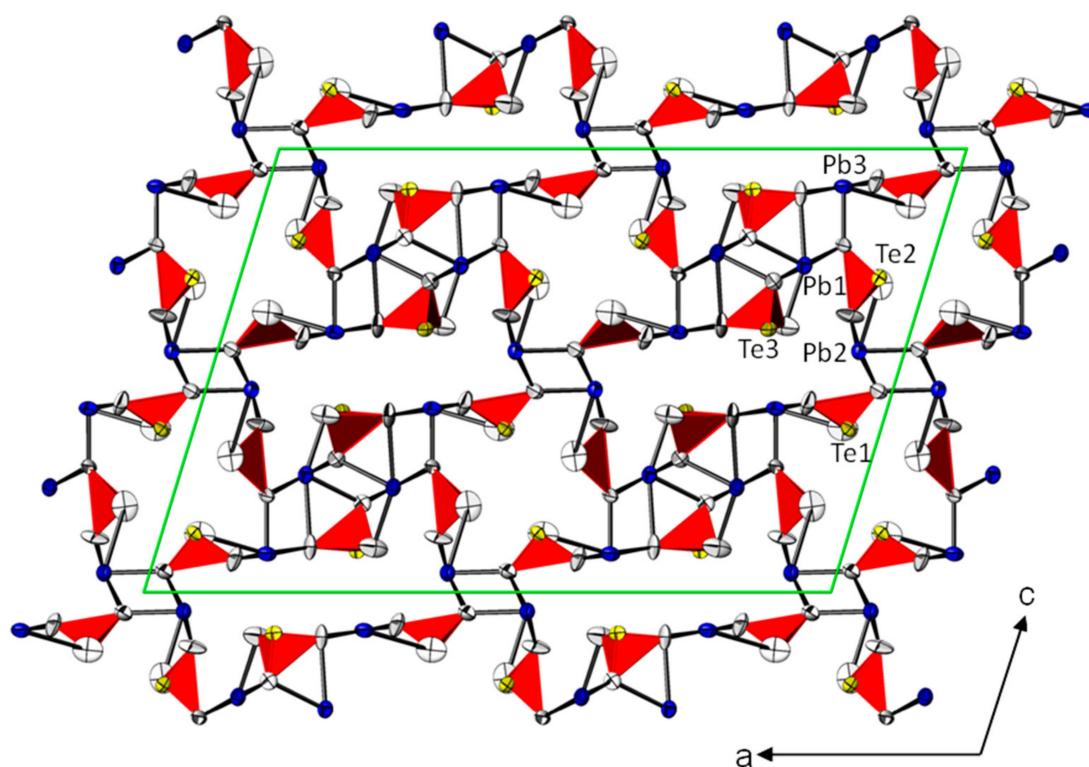

Figure 4. The crystal structure of α-PbTeO$_3$ in a projection along [010]. Colour codes and displacement ellipsoids are as in Figure 2. Crystal data were taken from the literature [6].

The results of BVS calculations for all three PbTeO$_3$ modifications are reasonably close to the expected values (in valence sums) of 2 for lead, 4 for tellurium, and 2 for oxygen atoms. Detailed values for γ- and β-PbTeO$_3$ are listed in Table 2 on the basis of the current structure refinements. Values for the Pb, Te, and O sites in the α-modification were calculated on the basis of the reported structure model [6] and range from 1.92–1.98, 3.92–4.03, and 1.63–2.18 valence units, respectively. The global instability index (GII) [26] can be used as a qualitative measure of the extent to which the valence sum rule is violated, and shows whether or not a structure is considered to be stable. Values of GII < 0.10 v.u. indicate that little or no strain is present in the crystal structure, values between 0.10 and 0.20 v.u. indicate a significant lattice-induced strain, and values > 0.20 v.u. suggest an instability of the structure due to too much strain. The calculated GII values of the three polymorphs amount to 0.07 v.u. for the γ-phase, 0.08 v.u. for the β-phase, and 0.15 v.u. for the α-phase. It should be noted that the GII values do not necessarily correlate with the thermodynamic stabilities of a given polymorphic compound, because metastable γ-PbTeO$_3$ has an even lower GII value than the thermodynamically stable β-form.

3.3. Raman Spectroscopy

Raman spectroscopic measurements were carried out with a sample obtained by precipitation (γ-form) and from samples obtained from DSC measurements after respective structural phase transitions and subsequent examination by powder X-ray diffraction (α- and β-forms). Raman spectra of the three $PbTeO_3$ polymorphs show a similar range of vibrational bands for the characteristic stretching and bending modes of the oxotellurate(IV) group (Figure 5).
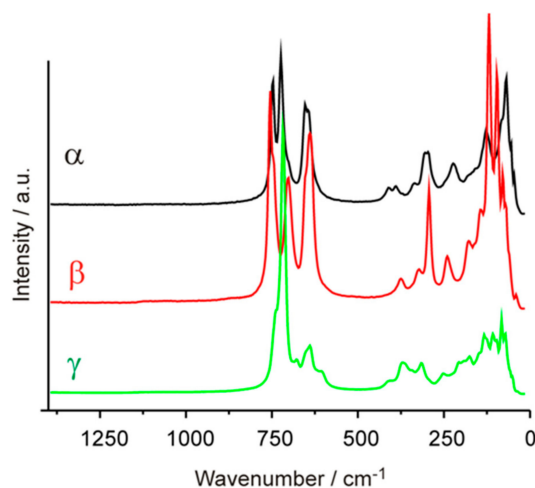

Figure 5. Raman spectra of the three $PbTeO_3$ polymorphs.

In a simplifying approximation, the corresponding trigonal-pyramidal TeO_3^{2-} anion can be treated to have C_{3V} symmetry in the solid state like it is in the free anion. Accordingly, four Raman-active modes—two *A*1 and two *E* modes—can be predicted [34], with vibrational bands centred around 760 and 700 cm^{-1} for the symmetric (ν_s) and anti-symmetric (ν_{as}) Te–O stretching vibrations, and around 360 and 330 cm^{-1} for the bending (δ) O–Te–O vibrations [35]. Correspondingly, for α-$PbTeO_3$ the symmetric stretching and anti-symmetric stretching vibrations are found at 747 and 724 cm^{-1}, and 654 and 645 cm^{-1}, respectively, and the bending vibrations at 411, 389, 336, 305, and 296 cm^{-1}. Analogous values for the two other modifications are β-$PbTeO_3$: 755 and 702 cm^{-1} (ν_s), 639 cm^{-1} (ν_{as}), 375, 322, 284 cm^{-1} (δ); γ-$PbTeO_3$: 738 and 718 cm^{-1} (ν_s), 679, 640, 606 cm^{-1} (ν_{as}), 403, 372, 345, 316 cm^{-1} (δ). These wave numbers are in agreement with those observed in the Raman spectra of other compounds comprising the TeO_3^{2-} anion; e.g., the synthetic thallium(I) compound Tl_2TeO_3 [36] or the mineral sonoraite $Fe^{III}Te^{IV}O_3(OH)·H_2O$ [37]. Raman bands in the region between 120 and 300 cm^{-1} observed for the three $PbTeO_3$ polymorphs can be associated with Pb–O modes, and at lower wave numbers with lattice vibrations. As noted above, the interpretation of the Raman bands associated with the TeO_3^{2-} anion is made on a simplifying approach. For each of the $PbTeO_3$ polymorphs, the TeO_3^{2-} anion deviates more or less from the idealized C_{3V} point group symmetry, leading to a splitting of bands in all cases. The presence of more than one TeO_3^{2-} group in the α- and γ-polymorphs additionally complicates matters. Although three and five TeO_3^{2-} groups, respectively, can be crystallographically distinguished for the latter two polymorphs, their Raman spectra are comparatively simple and show no remarkable broadening or a significant additional splitting of the vibrational bands. These features point to similar structural characteristics within and in the environment of each of the TeO_3^{2-} anions (Table 2; [6]).

3.4. Thermal Behaviour of γ-$PbTeO_3$

According to temperature-dependent X-ray powder diffraction measurements (Figure 6), γ-$PbTeO_3$ is stable in the oven chamber up to approximately 390 °C. At that temperature, the first reflections of the tetragonal β-polymorph appear. This is in agreement with the results of heating

experiments of precipitated material that was fired at 400 °C [11]. The transformation process γ-PbTeO$_3$ $\rightarrow$ β-PbTeO$_3$ is completed at about 450 °C. The β-polymorph in turn is stable up to 495 °C and then transforms into the α-polymorph. This phase remains stable in the oven chamber on direct cooling from 525 °C back to room temperature.
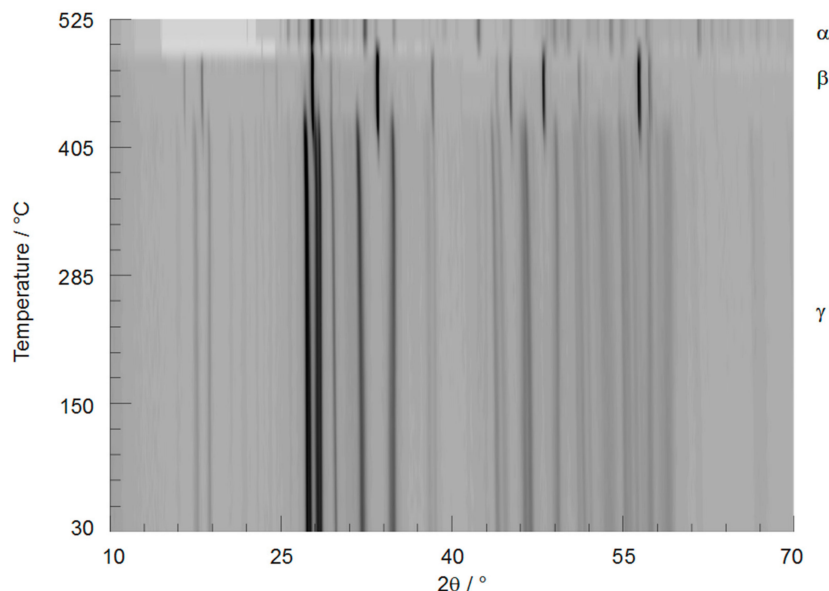

Figure 6. Temperature-dependent X-ray powder diffraction patterns of PbTeO$_3$ during heating in the range 30–525 °C. Assigned phases are given on the right.

The TG-curve (Figure 7) of γ-PbTeO$_3$ is in accordance with the phase transitions between the PbTeO$_3$ polymorphs and shows only a minute mass loss of less than 0.3% in the temperature range 25–500 °C. However, the nature of the released gaseous products remains undetermined. Since the main mass loss takes place at temperatures above 300 °C, it is unlikely that the released material originates from water molecules because chemi- or physisorbed water is usually desorbed at much lower temperatures, and therefore other volatile impurities might be responsible for the mass loss. For an unambiguous determination of the released material, future mass spectrometric measurements are required.
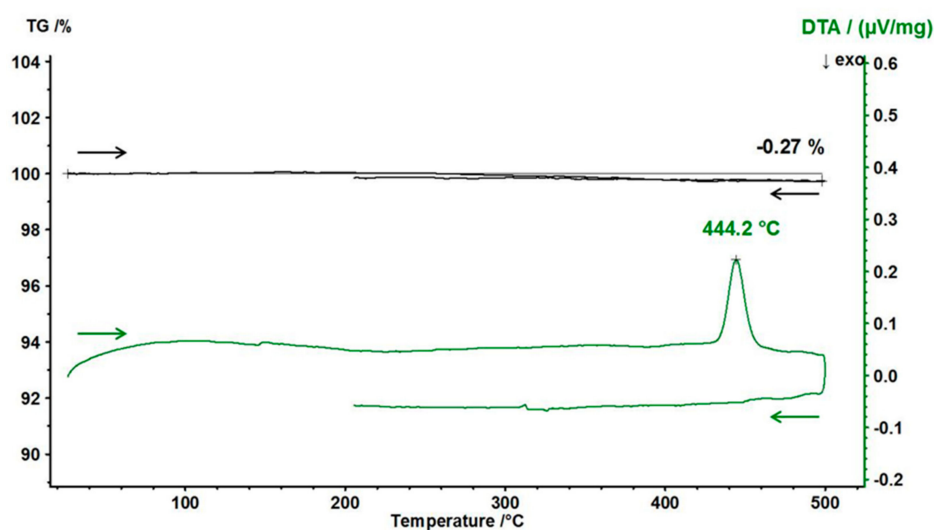

Figure 7. TG (black) and DTA (green) curves of γ-PbTeO$_3$ as starting material.

Several DSC measurements starting from γ-PbTeO$_3$ samples revealed a weak endothermic effect with onsets at about 440 °C. Values of peak maxima for the several runs are summarized in Table 3. This effect was clearly reproducible and was present only during the first heating cycle, thus pointing to an irreversible and monotropic behaviour (Figure 8).

Table 3. Peak maxima (°C) of the endothermal effects during heating of γ-PbTeO$_3$.

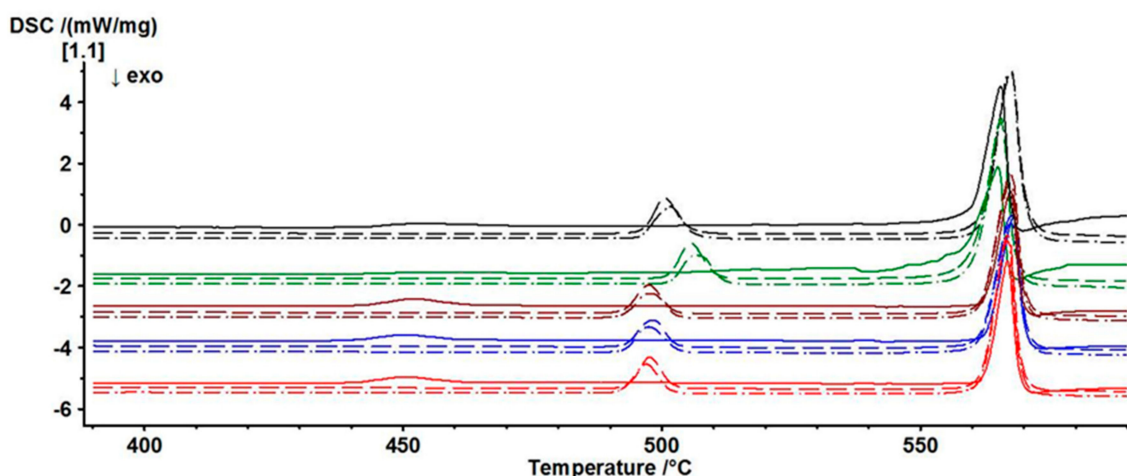| Measurement	Peak 1	Peak 2	Peak 3
1–1	453.8	—	565.6
1–2	—	500.5	567.5
1–3	—	501.8	567.4
2–1	455.8	—	565.0
2–2	—	505.7	565.5
2–3	—	506.5	565.6
3–1	452.3	—	567.6
3–2	—	497.4	567.5
3–3	—	497.6	567.3
4–1	450.6	—	568.0
4–2	—	498.3	567.6
4–3	—	497.4	567.5
5–1	450.6	—	566.9
5–2	—	497.7	566.9
5–3	—	496.9	566.8

Figure 8. Differential scanning calorimetry (DSC) results for five independent measurements of γ-PbTeO$_3$ including three heatings and coolings each (only heating curves are shown: first heating closed lines, second heating dashed lines, third heating dashed-dotted lines).

The product obtained from γ-PbTeO$_3$ samples heated up to 500 °C in the simultaneous thermal analyser (STA) or in several DSC measurements was always α-PbTeO$_3$ as revealed by ex-situ X-ray powder diffraction measurements at room-temperature. This finding (i.e., a direct transformation γ-PbTeO$_3 \rightarrow \alpha$-PbTeO$_3$) is in supposed contradiction to the results of temperature-dependent XRPD studies from which the above-deduced two-step mechanism would have been expected. We interpret the differences between the two analytical methods to be due to different time scales of the corresponding measurements and a concomitant kinetic control for the phase transitions. Whereas temperature-dependent XRPD measurements are slow due to stepwise heating rates and long measurement times for each temperature step, DSC measurements are much faster, with continuous heating rates and much shorter measurement times. Under the first conditions with longer heating times (which are comparable with the thermal treatment of precipitated material at 400 °C [11]),

formation of the β-polymorph is supported, whereas under conditions with shorter heating times formation of the α-polymorph is promoted. However, the γ-PbTeO$_3$ → α-PbTeO$_3$ transformation is sluggish and is accompanied with a very weak endothermal effect.

We have additionally investigated γ-PbTeO$_3$ samples by DSC measurements including melting and re-crystallization. For that purpose, both one-cycle measurements (RT → 590 °C → RT) and multi-cycle measurements with up to three single cycles were performed. The corresponding thermal behaviour appears likewise to be kinetically controlled. When heated above the γ-PbTeO$_3$ → α-PbTeO$_3$ transition, the material melts at 566(2) °C (onset of several measurements; Table 4) and recrystallizes with a great hysteresis at much lower temperatures. The recrystallisation temperature—indicated by a strong exothermal effect—is very variable, with maximum and minimum onset temperatures of ca. 510 °C and 460 °C. In the majority of cases, the recrystallized material obtained at room temperature was β-PbTeO$_3$, but in few cases α-PbTeO$_3$ had formed as a single phase after the first heating cycle. Which of the two polymorphs is eventually formed after recrystallization depends on formation of respective seed crystals, and points to only small thermodynamic differences between α- and β-PbTeO$_3$. In the case of multiple heating and cooling cycles including melting, the derived melting points remain constant within the usual standard deviation and are the same as for single heating/cooling cycles (see above). Again, recrystallisation for several heating cycles starts both with a great hysteresis and with different temperatures. Figure 9 shows a typical multi-heating/cooling cycle DSC measurement.

Table 4. Peak maxima (°C) during three subsequent heating/cooling cycles of γ-PbTeO$_3$ as starting material.

Measurement	Peak 1	Peak 2	Peak 3
1–1 (heating)	453.7	—	565.6
1–2 (cooling)			492.3
2–1 (heating)	—	500.5	567.5
2–2 (cooling)			497.9
3–1 (heating)	—	501.8	567.4
3–2 (cooling)			481.0

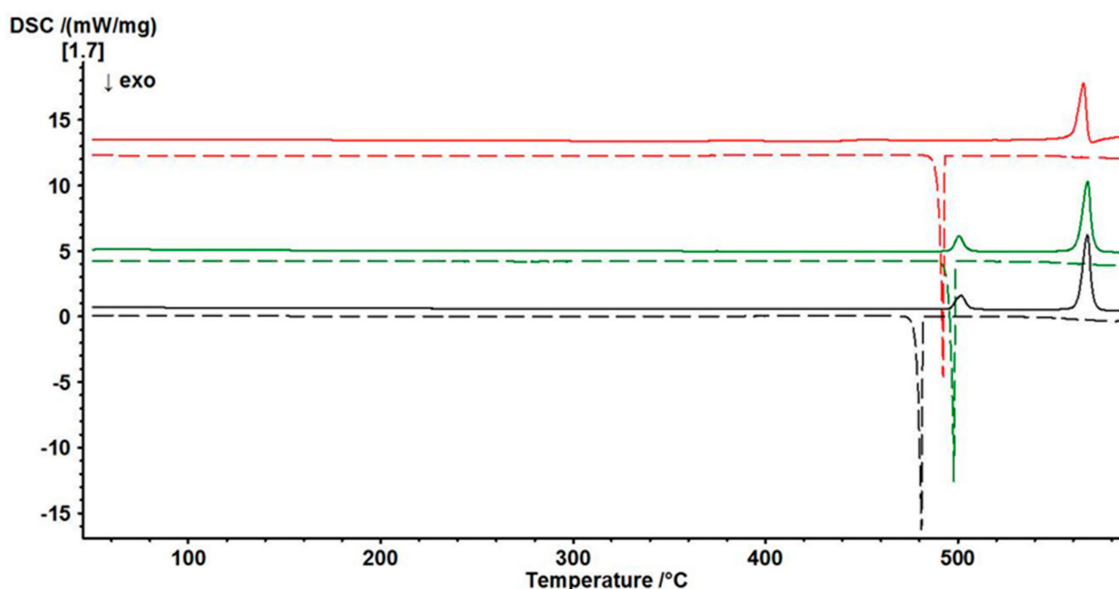**Figure 9.** DSC measurements with multiple heating/cooling cycles of an identical γ-PbTeO$_3$ sample, starting from γ-PbTeO$_3$ (temperature range 25–590 °C). Heatings are shown with closed lines, coolings with dashed lines. First cycle (red), second cycle (green), third cycle (black).

As can be seen, the first heating cycle includes the very weak and sluggish γ-PbTeO$_3$ $\rightarrow$ α-PbTeO$_3$ transition at about 440 °C, that—after melting and recrystallisation of β-PbTeO$_3$—is missing in the second heating cycle. Instead, a much stronger endothermic effect occurs at 490 °C (onset), which indicates the β-PbTeO$_3$ $\rightarrow$ α-PbTeO$_3$ transition. This effect is reproducible (see third heating cycle), provided the β-polymorph had again formed after recrystallization.

4. Conclusions

Conflicting results in the literature about the water content of "hydrous PbTeO$_3$" were resolved. In fact, this phase does not contain any structural water, as revealed by crystal structure determination from single crystal X-ray data, vibrational spectroscopy, and thermogravimetry. This phase actually represents a third PbTeO$_3$ polymorph, denoted as the γ-form. Upon heating, the latter shows an irreversible phase transition into one of the other two polymorphs (α- or β-). Which of the two polymorphs is eventually formed appears to be kinetically controlled. Slow heating with longer holding times led to the β-polymorph (heating in an oven; temperature-dependent X-ray diffraction), whereas faster and continuous heating rates (DSC measurements) produced the α-form, accompanied by a very weak endothermal effect. DSC measurements including melting and recrystallisation indicate an enantiotropic behaviour for the β-PbTeO$_3$ $\rightarrow$ α-PbTeO$_3$ transformation.

Author Contributions: Matthias Weil conceived and designed this study and also performed experiments related to diffraction methods and wrote the paper; Mahdi Shirkhanlou performed crystal growth experiments; Ekkehard Füglein performed thermal analysis studies; Eugen Libowitzky performed spectroscopic studies.

Conflicts of Interest: The authors declare no conflict of interest.

References

1. Galy, J.; Meunier, G.; Andersson, S.; Åström, A. Stéréochimie des eléments comportant des paires non liées: Ge(II), As(III), Se(IV), Br(V), Sn(II), Sb(III), Te(IV), I(V), Xe(VI), Tl(I), Pb(II), et Bi(III) (oxydes, fluorures et oxyfluorures). *J. Solid State Chem.* **1975**, *13*, 142–159. [CrossRef]
2. Shimoni-Livny, L.; Glusker, J.P.; Bock, C.W. Lone pair functionality in divalent lead compounds. *Inorg. Chem.* **1998**, *37*, 1853–1867. [CrossRef]
3. Kosse, L.I.; Politova, E.D.; Bush, A.A.; Astaf'ev, A.V.; Stefanovich, S.Y.; Myzgin, E.A.; Venevtsev, Y.N. Growing and some properties of β-PbTeO$_3$ monocrystals. *Kristallografiya* **1983**, *28*, 510–513.
4. Sciau, P.; Lapasset, J.; Moret, J. Structure de la phase quadratique de PbTeO$_3$. *Acta Crystallogr.* **1986**, *42*, 1688–1690. [CrossRef]
5. Mariolacos, K. Die Kristallstruktur von PbTeO$_3$. *Anzeiger der Österreichische Akademie der Wissenschaften Mathematisch-Naturwissenschatliche Klasse* **1969**, *106*, 129–130.
6. Zavodnik, V.E.; Ivanov, S.A.; Stash, A.I. α-Lead tellurite from single-crystal data. *Acta Crystallogr.* **2008**, *64*, 16. [CrossRef] [PubMed]
7. Williams, S.A. Girdite, Oboyerite, Fairbankite, and Winstanleyite, Four New Tellurium Minerals from Tombstone, Arizona. *Mineral. Mag.* **1979**, *43*, 453–457. [CrossRef]
8. Spiridonov, E.M.; Tananeyva, O.I. Plumbotellurite, α-PbTeO$_3$, a new mineral. *Doklady Akademii Nauk SSSR* **1982**, *262*, 1231–1235.
9. Gaitan, M.; Jerez, A.; Noguerales, P.; Pico, C.; Veiga, M.L. New Methods of synthesis of mixed oxides of Te and Pb: characterization of the new phases PbTeO$_3$ (cubic) and PbTeO$_4$ (orthorhombic). *Synth. React. Inorg. Met–Org. Chem.* **1987**, *17*, 479–490. [CrossRef]
10. Tananaeva, O.I.; Latypova, Z.K.; Novoselova, A.V. Study of PbTe-PbTeO$_3$ and PbTeO$_4$-PbO cross-sections of Pb-Te-O system. *Izvestiya Akademii Nauk SSSR Neorganicheskie Materialy* **1977**, *13*, 386–387.
11. Young, I.M. The central region of the PbO/TeO$_2$ phase diagram. *J. Mater. Sci.* **1979**, *14*, 1579–1585. [CrossRef]
12. Stavrakieva, D.; Ivanova, Y.; Pyrov, J. On the composition of the crystal phases in the PbO-TeO$_2$ system. *J. Mater. Sci.* **1988**, *23*, 1871–1876. [CrossRef]

13. Sootsman, J.R.; Chung, D.Y.; Kanatzidis, M.G. New and old concepts in thermoelectric materials. *Angew. Chem. Int. Ed.* **2009**, *48*, 8616–8639. [CrossRef] [PubMed]

14. Berchenko, N.; Fadeev, S.; Savchyn, V.; Kurbanov, K.; Trzyna, M.; Cebulski, J. Pb–Te–O phase equilibrium diagram and the lead telluride thermal oxidation. *Thermochim. Acta* **2014**, *579*, 64–69. [CrossRef]

15. El-Rabaie, S.; Taha, T.A.; Higazy, A.A. PbTe quantum dots formation in a novel germanate glass. *J. Alloys Compd.* **2014**, *594*, 102–106. [CrossRef]

16. Scheele, M.; Oeschler, N.; Veremchuk, I.; Peters, S.O.; Littig, A.; Kornowski, A.; Klinke, C.; Weller, H. Thermoelectric properties of lead chalcogenide core–shell nanostructures. *ACS Nano* **2011**, *5*, 8541–8551. [CrossRef] [PubMed]

17. Gopalakrishnan, J. Chimie douce approaches to the synthesis of metastable oxide materials. *Chem. Mater.* **1995**, *7*, 1265–1275. [CrossRef]

18. Stöger, B.; Weil, M.; Baran, E.J.; González-Baró, A.C.; Malo, S.; Rueff, J.M.; Petit, S.; Lepetit, M.B.; Raveau, B.; Barrier, N. The dehydration of $SrTeO_3(H_2O)$—A topotactic reaction for preparation of the new metastable strontium oxotellurate(IV) phase ε-$SrTeO_3$. *Dalton Trans.* **2011**, *40*, 5538–5548. [CrossRef] [PubMed]

19. Tananaeva, O.I.; Novoselova, A.V. Thermal stability of lead tellurite(IV) and tellurate(VI). *Izvestiya Akademii Nauk SSSR Neorganicheskie Materialy* **1967**, *3*, 114–118.

20. Berchenko, M.A.; Belyaev, A.I. Preparation of lead, barium, and copper tellurites by precipitation from solution. *Zhurnal Neorganicheskoi Khimii* **1967**, *12*, 1774–1781.

21. Champarnaud-Mesjard, J.C.; Thomas, P.; Colas-Dutreilh, M.; Oufkir, A. Crystal structure of dilead tritellurate (IV), $Pb_2Te_3O_8$. *Z. Kristallogr. New Cryst. Struct.* **2001**, *216*, 185–186.

22. Artner, C.; Weil, M. Re-examination of "Pb_3TeO_6": Determination of its correct composition as Pb_5TeO_8. *J. Solid State Chem.* **2013**, *199*, 240–247. [CrossRef]

23. *APEX-2, SAINT and SADABS*; Bruker AXS Inc.: Madison, WI, USA, 2013.

24. Sheldrick, G.M. A short history of SHELX. *Acta Crystallogr.* **2008**, *64*, 112–122. [CrossRef] [PubMed]

25. Herrendorf, W. *HABITUS*; Universities of Karlsruhe and Gießen: Karlsruhe, Germany, 1997.

26. Brown, I.D. *The Chemical Bond in Inorganic Chemistry: The Bond Valence Model*; Oxford University Press: Oxford, UK, 2002.

27. Krivovichev, S.V.; Brown, I.D. Are the compressive effects of encapsulation an artifact of the bond valence parameters? *Z. Kristallogr.* **2001**, *216*, 245–247. [CrossRef]

28. Brown, I.D.; Altermatt, D. Bond-Valence parameters obtained from a systematic analysis of the inorganic crystal structure database. *Acta Crystallogr.* **1985**, *41*, 244–247. [CrossRef]

29. Dowty, E. *ATOMS for Windows*, Version 6.3; Shape Software: Kingsport, TN, USA, 2006.

30. Christy, A.G.; Mills, S.J.; Kampf, A.R. A review of the structural architecture of tellurium oxycompounds. *Mineral. Mag.* **2016**, *80*, 415–545. [CrossRef]

31. Zemann, J. Zur Stereochemie des Te(IV) gegenüber Sauerstoff. *Monatsh. Chem.* **1971**, *102*, 1209–1216. [CrossRef]

32. Bondi, A. Van der waals volumes and radii. *J. Phys. Chem.* **1964**, *68*, 441–451. [CrossRef]

33. Parsons, S.; Flack, H.D.; Wagner, T. Use of intensity quotients and differences in absolute structure refinement. *Acta Crystallogr.* **2013**, *69*, 249–259. [CrossRef] [PubMed]

34. Weidlein, J.; Müller, U.; Dehnicke, K. *Schwingungsspektroskopie*; Thieme Verlag Press: Stuttgart, Baden-Württemberg, Germany, 1988.

35. Farmer, V.C. (Ed.) *Mineralogical Society Monograph 4: The Infrared Spectra of Minerals*; The Mineralogical Society Press: London, UK, 1974.

36. Rieger, F.; Mudring, A.V. Phase Transition in Tl_2TeO_3: Influence and origin of the thallium lone pair distortion. *Inorg. Chem.* **2007**, *46*, 446–452. [CrossRef] [PubMed]

37. Frost, R.L.; Keeffe, E.C. Raman spectroscopic study of the tellurite mineral: Sonoraite $Fe^{3+}Te^{4+}O_3(OH) \cdot H_2O$. *J. Raman Spectrosc.* **2009**, *40*, 133–136. [CrossRef]